Soft Matter

PAPER

View Article Online
View Journal | View Issue

Cite this: *Soft Matter*, 2022, 18, 4679

New patterns of twist-bend liquid crystal phase behaviour: the synthesis and characterisation of the 1-(4-cyanobiphenyl-4′-yl)-10-(4-alkylaniline-benzylidene-4′-oxy)decanes (CB10O·*m*)†

Ahlam F. Alshammari, ‡[a] Damian Pociecha,[b] Rebecca Walker,[a] John M. D. Storey,[a] Ewa Gorecka[b] and Corrie T. Imrie *[a]

Received 1st February 2022,
Accepted 28th May 2022

DOI: 10.1039/d2sm00162d

rsc.li/soft-matter-journal

The synthesis and characterisation of the 1-(4-cyanobiphenyl-4′-yl)-10-(4-alkylanilinebenzylidene-4′-oxy)decanes (CB10O·*m*) are reported. This series shows a rich liquid crystal polymorphism including twist-bend nematic and smectic phases. All the homologues reported exhibit an enantiotropic conventional nematic phase. For the homologues with $m \leq 10$, the local packing in the nematic phases and the layer spacing in the smectic phases indicates an intercalated arrangement of the molecules. An intercalated smectic C_A phase is observed if $m/11 \approx 0.5$. Either side of this condition, the twist-bend nematic phase is observed, a novel pattern of behaviour for a series on increasing a terminal chain length. For longer chain lengths, m = 12, 14, 16 and 18, two twist-bend smectic C (SmC_{TB}) phases are observed, and the packing of the molecules is now of a bilayer-type. The higher temperature variant is termed $SmC_{TB\text{-}SH}$ in which SH (single helix) refers to the presence of a short, distorted clock-type helix. In the lower temperature $SmC_{TB\text{-}DH}$ phase, an additional longer helix is superimposed on the short one, and DH denotes double helix.

Introduction

Heliconical liquid crystal phases formed by achiral molecules constitute the newest class of liquid crystal phases and have attracted considerable global research interest. The simplest of these phases is the twist-bend nematic (N_{TB}) phase, first identified some ten years ago for the odd-membered liquid crystal dimer CB7CB[1–3] and a decade after a prediction was made by Dozov that bent molecules should exhibit both twist-bend nematic and smectic phases.[4] In the N_{TB} phase, the director forms a helix and is tilted with respect to the helical axis, and this was the first example of spontaneous chiral symmetry breaking in a fluid with no positional order. The spontaneous formation of chirality ensures that equal numbers of left- and right-handed helices are formed, but if the constituent molecules are chiral, this degeneracy is removed and the chiral N_{TB} phase is obtained.[5] More recently, heliconical twist-bend smectic C (SmC_{TB}) phases have also been discovered for liquid crystal dimers[6,7] and in bent-core mesogens.[8,9] It appears that a range of variants of this phase, similar to the SmC* subphases observed for chiral molecules, are possible.[10]

The key structural requirement for the observation of the N_{TB} phase is a bent molecular structure and this is most often realised using odd-membered liquid crystal dimers. These consist of molecules containing two mesogenic groups connected by a spacer having an odd number of atoms (see, for example, ref. 11–29) although other structures such as higher oligomers,[30–36] semi-rigid bent core liquid crystals,[37,38] and hydrogen-bonded systems[39–43] are also known to support the formation of the N_{TB} phase. The search for the twist-bend smectic phases has also been focussed on bent mesogenic dimers, but in order to drive smectic phase formation, the molecular design must also incorporate molecular inhomogeneity. This was achieved using non-symmetric liquid crystal dimers having different mesogenic units.[44] It is known that if the mesogenic units in such structures are selected in order to exhibit a specific, favourable interaction then depending on the ratio of the length of the flexible spacers and terminal chains, a range of smectic phases may be observed including intercalated and interdigitated variants.[45–48] Using this design strategy, examples of the SmC_{TB} phase have been found for members of the CB*n*O·*m* series, see Fig. 1, with n = 6 and m = 10–12, 14,

[a] *Department of Chemistry, School of Natural and Computing Sciences, University of Aberdeen, AB24 3UE Scotland, UK. E-mail: c.t.imrie@abdn.ac.uk*
[b] *University of Warsaw, Faculty of Chemistry, ul. Zwirki i Wigury 101, 02-089 • Warsaw, Poland*

† Electronic supplementary information (ESI) available. See DOI: https://doi.org/10.1039/d2sm00162d

‡ Permanent address: Department of Chemistry, University of Hail, Hail, Saudi Arabia.

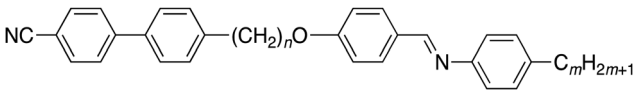

Fig. 1 The general molecular structure of the CB*n*O·*m* series. The dimers reported here have n = 10, and m = 1–10, 12, 14, 16, 18.

16, and 18.[7,10,49] For terminal chain lengths with $m < 10$, twist-bend and conventional nematic phases are observed but no smectic behaviour is seen. By analogy with other non-symmetric dimer series,[50] if the terminal chain in a CB*n*O·*m* series was significantly shorter than the spacer length then smectic behaviour should emerge, and to investigate this intriguing possibility here we report the synthesis and characterisation of the 1-(4-cyanobiphenyl-4′-yl)-10-(4-alkylanilinebenzylidene-4′-oxy)decanes (Fig. 1, n = 10), in which we extend the length of the terminal chain. The decyloxy spacer has been previously shown to endow the required molecular curvature for the N_{TB} phase to be observed.[51]

Experimental

Synthesis

The synthetic route used to obtain the CB10O·*m* series is shown in Scheme 1. The convenient synthesis of 10-bromo-1-(4-cyanobiphenyl-4′-yl) decane based on a sodium mediated aromatic cross-coupling reaction has been described in detail elsewhere.[52] Complete synthetic details, structure and purity characterisation data for the final products and along with their intermediates are provided in the ESI.†

Thermal characterisation

The phase behaviour of the complexes was studied by differential scanning calorimetry (DSC) using a Mettler-Toledo DSC1 fitted with an intracooler and calibrated using indium and zinc as standards. The thermograms were obtained during heating and cooling scans at 10 °C min^{-1}, under a nitrogen atmosphere. All samples were measured in duplicate. Transition temperatures and associated enthalpy changes were extracted from the second-heating trace, unless otherwise stated, and those listed are an average for both samples measured. The transition temperatures were assigned as the maximum of the heat flow associated with the transition.

X-Ray diffraction

The small angle X-ray diffraction (SAXS) patterns for powder samples were obtained with a Bruker Nanostar system using CuKα radiation and patterns were collected with an area detector VANTEC2000. The temperature of the sample was controlled with precision of ±0.1 K. Wide angle diffractograms (WAXS) were obtained with a Bruker D8 GADDS system (CuKα line, Goebel mirror, point beam collimator, VANTEC2000 area detector). Samples were prepared as droplets on a heated surface.

Polarized light microscopy and birefringence measurements

Observations of optical textures were performed using a Zeiss AxioImager A2m microscope equipped with a Linkam heating stage. Samples were prepared either in commercially available cells (provided by Warsaw Military University of Technology, WAT), having 1.6–5 micron thickness, and polymer aligning layers for planar or homeotropic anchoring; in addition, samples prepared between untreated glass slides and one-free-surface samples were used. Birefringence was measured with a setup based on a photoelastic modulator (PEM-90, Hinds) working at a modulation frequency f = 50 kHz; as a light source, a halogen lamp (Hamamatsu LC8) was used equipped with narrow bandpass filters (633 nm and 690 nm). The signal from a photodiode (FLC Electronics PIN-20) was deconvoluted with a lock-in amplifier (EG&G 7265) into 1f and 2f components to yield a retardation induced by the sample. Knowing the sample thickness, the retardation was recalculated into optical birefringence. Samples were prepared in 3-micron-thick cells with planar anchoring. The alignment quality was checked prior to measurement by inspection under the polarised light optical microscope.

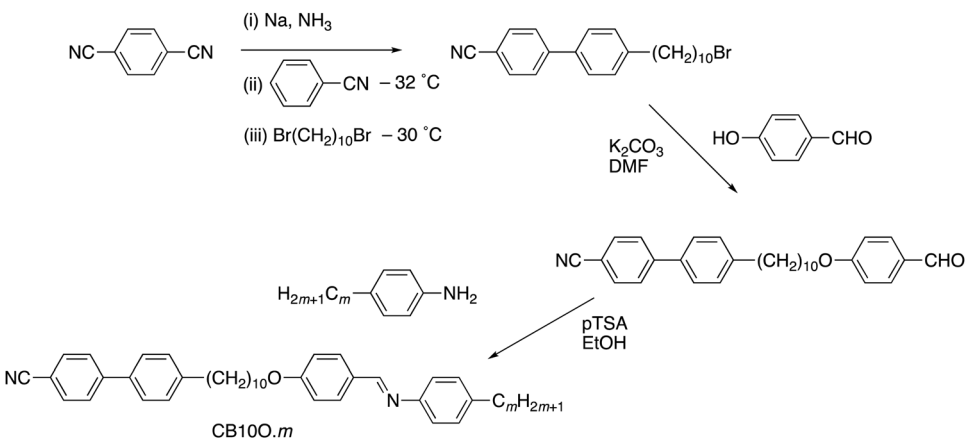

Scheme 1

Results and discussion

The dependence of the transition temperatures on the length of the terminal chain for the CB10O·*m* series is shown in Fig. 2, and the associated transitional data are provided in the ESI,† Table S1. The CB10O·*m* series exhibits a rich phase polymorphism including the N and N_{TB} phases, and up to six smectic phases including twist-bend variants. All the homologues prepared exhibited an enantiotropic conventional nematic (N) phase identified using polarised light microscopy, and based on the observation of a characteristic schlieren texture containing both two and four brush point singularities and which flashed when subjected to mechanical stress when sandwiched between untreated glass slides. The N phase exhibited a uniform texture when viewed in a cell treated for planar anchoring. On cooling the N phase for the homologues with m = 1–3, 7–10, 12 and 14, the schlieren texture changed to give a striated schlieren with regions of rope-like texture between untreated glass slides (Fig. 3), and a striped texture in planar cells. In addition, the optical flickering associated with director fluctuations in the nematic phase ceased at the transition. These observations are consistent with an N–N_{TB} transition. On cooling the N_{TB} phase for CB10O.2 a mosaic texture formed at the transition to the smectic X phase, see Fig. 3(c). By contrast, on cooling the N phase for m = 4–6, a focal conic fan texture developed, and when sheared, a weakly birefringent schlieren texture was obtained containing both, two- and four-brush point defects, indicating an anticlinic smectic C_A phase, see Fig. 4. The focal conic-fan texture remained essentially unchanged on entering the SmX phase whereas the schlieren texture became less well-defined. Cooling the N_{TB} phase shown by m = 3, 7 and 8 gave similar textures indicating the formation of a SmC_A phase. On cooling the N_{TB} phase seen for m = 9 and 10, no changes were observed prior to crystallisation.

X-Ray diffraction studies confirmed these phase assignments. The diffraction patterns of the N and N_{TB} phases are essentially identical, and only broad signals were observed in both the low and wide-angle regions indicative of the liquid-like arrangement of the molecules, see Fig. 5. The local periodicities in the nematic phase for m = 1–10, deduced from the position of the peak in the low angle region, corresponded to about half the molecular length, l, strongly suggesting that the short-range structure in these phases is an intercalated arrangement. The diffraction patterns for the SmC_A phase contained a sharp reflection in the low angle region implying a layered structure, and a broad peak in the wide-angle indicative of the liquid-like

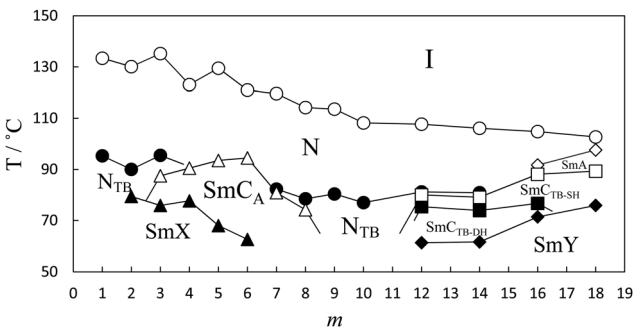

Fig. 2 The dependence of the transition temperatures on the number of carbon atoms in the terminal chain for the CB10O·*m* series. The melting points have been omitted for the sake of clarity.

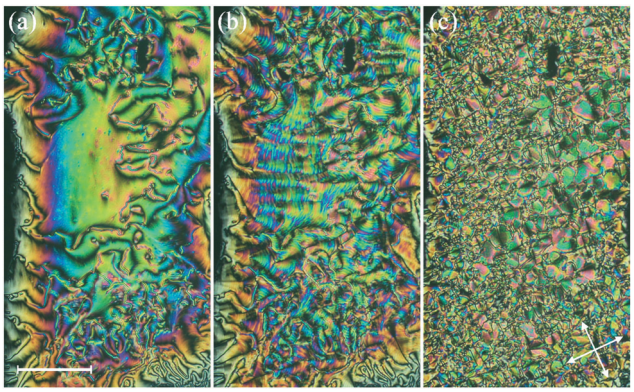

Fig. 3 The optical textures observed for (a) nematic (T = 110 °C), (b) twist-bend nematic (T = 92 °C), and (c) smectic X (T = 75 °C) phases shown by CB10O·2. The scale bar corresponds to 100 μm, arrows show directions of crossed polarizers.

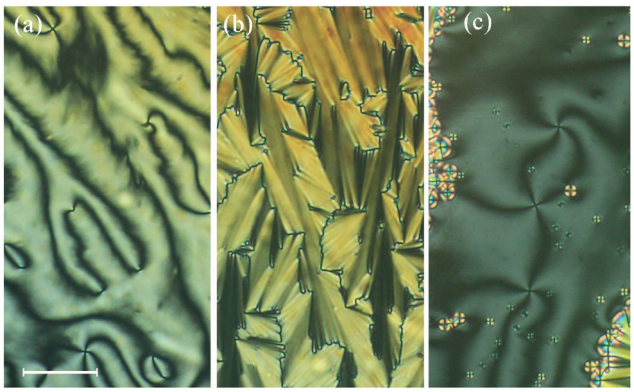

Fig. 4 (a) The schlieren texture of the nematic phase (T = 100 °C), (b) the focal conic texture and (c) the schlieren texture obtained after shearing the smectic C_A phase (T = 87 °C) seen for CB10O·5. The scale bar corresponds to 20 μm.

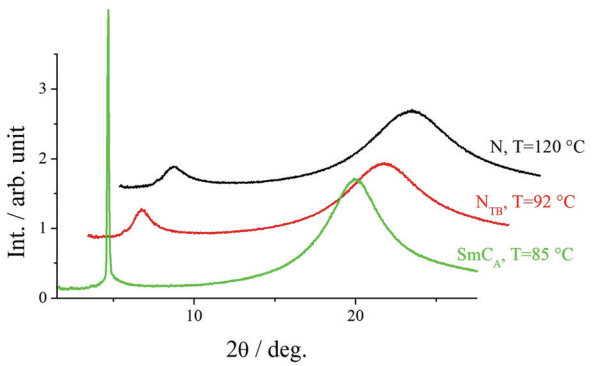

Fig. 5 Intensity profiles for the X-ray diffraction patterns of the N, N_{TB} and SmC_A phases shown by CB10O·3.

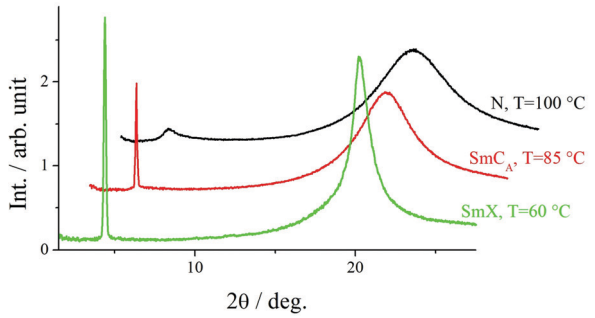

Fig. 6 Intensity profiles for the X-ray diffraction patterns of the N, SmC_A and SmX phases shown by CB10O·5.

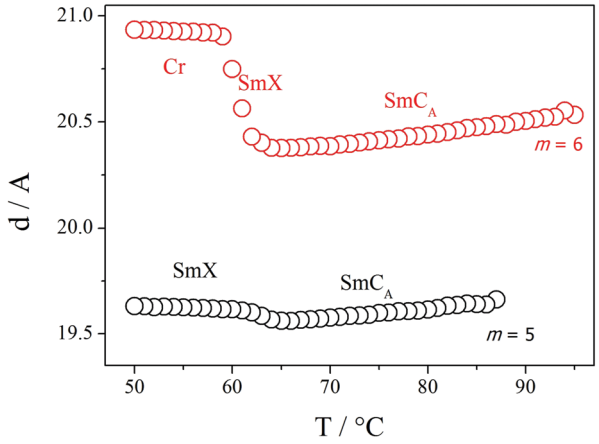

Fig. 8 The temperature dependence of the layer spacing for the smectic phases shown by CB10O·5 (black) and CB10O·6 (red).

arrangement of the molecules within the layers, see Fig. 5 and 6. The layer spacing, d, in the smectic C_A phase is approximately half the molecular length consistent with an intercalated arrangement of the molecules, see Fig. 7. In the SmX phase, the wide-angle signal narrows considerably, see Fig. 6, evidencing a substantial growth in the correlation length of the positional order of the molecules within the layers, and this is typical for hexatic type phases.[53] The strongly monotropic nature of the SmX phase prevented its further study. The temperature dependence of the layer spacing in the smectic phases shown by m = 5 and 6 is shown in Fig. 8. A weak temperature dependence is observed with a positive thermal expansion coefficient in the SmC_A phase of the order of 0.005 Å K^{-1}, which is consistent with the tilted character of the phase. Fig. 9 shows the intensity profiles for the X-ray diffraction patterns of the N and N_{TB} phases shown by CB10O·9 and as noted earlier, in both phases the short-range structure is intercalated.

We now turn our attention to the longer homologues of the series with m = 12, 14, 16 and 18. On cooling the N phase for m = 12 and 14, at the first transition, the texture becomes blocky and defects develop. On further cooling these defects become more pronounced and the texture develops fan-like regions at the second transition. In a cell treated for planar alignment a uniform texture is observed in the N phase, and in the N_{TB} phase a rather weak striped texture develops which becomes more pronounced at the consecutive transitions (Fig. 10). For one-free-surface samples, a sequence of schlieren–homeotropic–schlieren–homeotropic textures was seen (Fig. 10(e–h)), suggesting two of these phases to be optically uniaxial. Fig. 11 shows the intensity profiles for the X-ray diffraction patterns obtained for the two higher temperature smectic phases seen for CB10O·12, and in both, sharp signals are observed in the low angle region arising from the layered structure, and only a broad signal is seen in the wide angle range indicating the liquid-like nature of the molecules within the layers. For these smectic phases the layer spacing is approximately twice the molecular length suggesting an interdigitated bilayer-type arrangement. On cooling the $SmC_{TB\text{-}DH}$ phase, the high angle signal in the diffraction starts to narrow and split in the SmY phase.

On cooling the N phase for m = 16 and 18, the sample became optically extinct when viewed as a one-free-surface sample, see Fig. 12, and in a cell treated for planar alignment, the optical flickering ceased, indicating a smectic A (SmA) phase. In the nematic phase shown by CB10O·16, the local periodicity deduced from the position of the diffuse peak in the low angle region, varied from 82 to 88 Å on cooling towards the transition to the smectic phase, and this corresponds to about twice the molecular length strongly suggesting a short-range bilayer structure. The X-ray diffraction pattern of the SmA phase consisted of a sharp signal in the low angle region implying a layered structure, and in the wide angle a broad peak arising from the liquid-like arrangement of the molecules

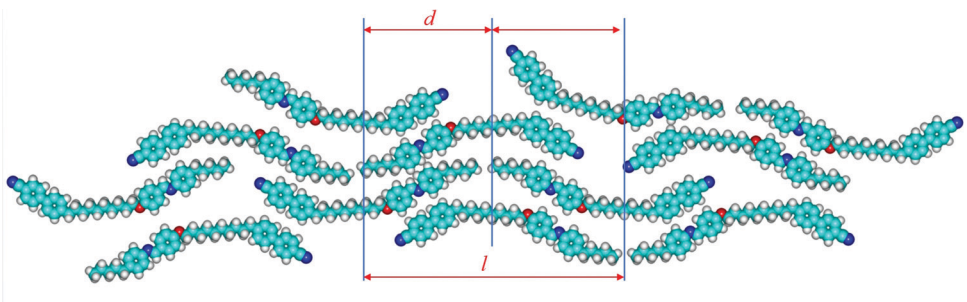

Fig. 7 A sketch of the intercalated smectic C_A phase exhibited by the CB10O·m series with m = 3–8. The ratio of the layer spacing, d, to the molecular length, l, is approximately 0.5. The molecular geometry was optimised using HyperChem software.

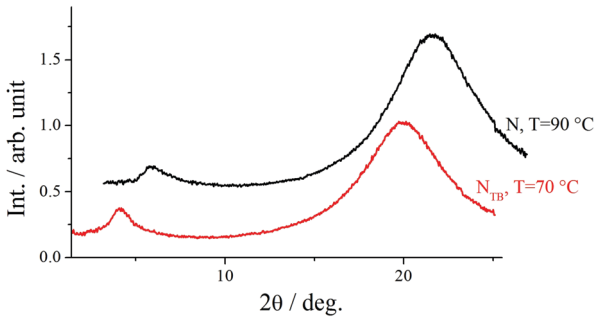

Fig. 9 Intensity profiles for the X-ray diffraction patterns of the N, and N_{TB} phases shown by CB10O·9.

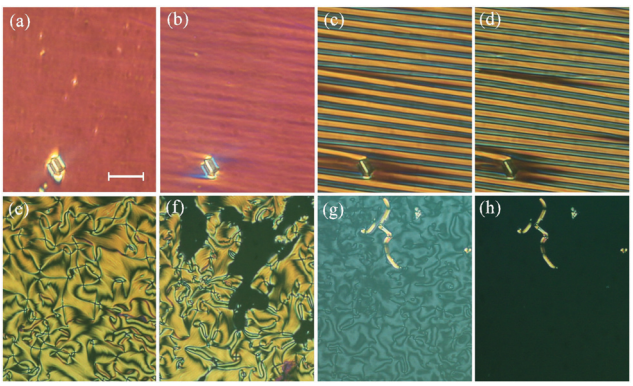

Fig. 10 The textures seen for CB10O·12 on cooling from the isotropic phase in (upper row) a cell treated for planar alignment in (a) N (107 °C), (b) N_{TB} (81 °C), (c) $SmC_{TB\text{-}SH}$ (78 °C), and (d) $SmC_{TB\text{-}DH}$ (73 °C) phases, and (lower row) for a one-free-surface sample in (e) N (105 °C) (f) at the N–N_{TB} transition (81 °C), (g) $SmC_{TB\text{-}SH}$ (77 °C), and (h) $SmC_{TB\text{-}DH}$ (71 °C) phases. The scale-bar corresponds to 20 μm.

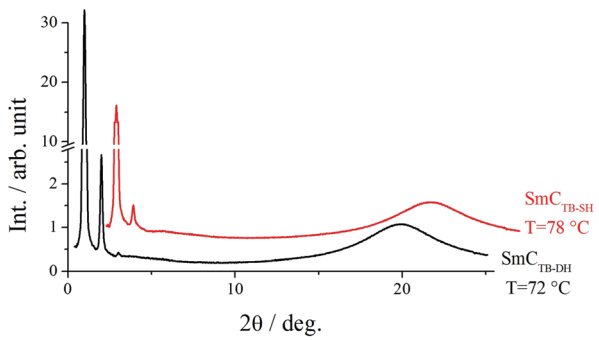

Fig. 11 Intensity profiles for the X-ray diffraction patterns of the $SmC_{TB\text{-}SH}$ and $SmC_{TB\text{-}DH}$ phases shown by CB10O·12. Crystallisation precluded the measurement of a good quality pattern in the SmY phase.

within a layer. The layer spacing was approximately twice the molecular length. On cooling the smectic A phase, a dynamic schlieren texture was observed for a one-free surface sample that on further cooling, became homeotropic suggesting the formation of a uniaxial phase, see Fig. 12. In a cell treated for planar alignment, faint lines appeared on cooling the smectic A phase which became stronger on further cooling. These changes on cooling from the homeotropic SmA texture to a dynamic

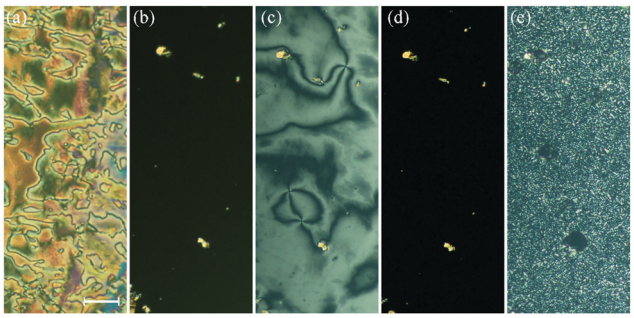

Fig. 12 The optical textures seen for CB10O·16 on cooling from the isotropic phase for a one-free-surface sample in the (a) N (101 °C), (b) SmA (90 °C), (c) $SmC_{TB\text{-}SH}$ (80 °C), (d) $SmC_{TB\text{-}DH}$ (72 °C), and (e) SmY (68 °C) phases. The scale-bar corresponds to 20 μm.

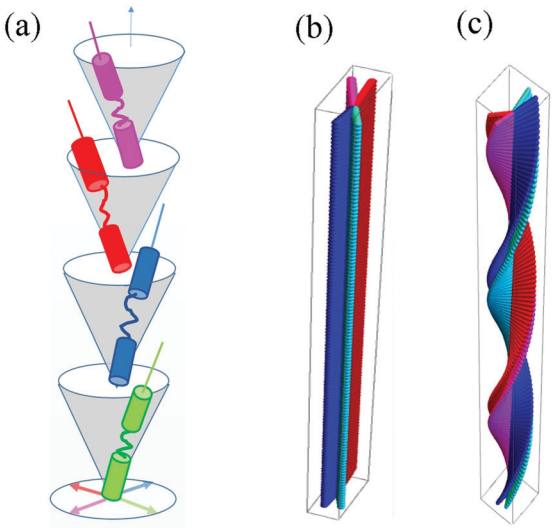

Fig. 13 (a) A sketch of the basic, four-layer unit of a SmC_{TB} phase with a distorted-clock structure; the molecules in consecutive layers change their azimuthal position on a tilt cone. Projections of the molecules on the smectic planes in the (b) $SmC_{TB\text{-}SH}$ and (c) $SmC_{TB\text{-}DH}$ phases, the presence of an additional helix in the $SmC_{TB\text{-}DH}$ makes the structure optically uniaxial.

schlieren texture and back to a homeotropic texture suggests a sequence of SmC_{TB} phases similar to that we have recently described for CB6O·*m* homologues having long terminal chains,[10] and shown schematically in Fig. 13. The higher temperature of these phases is termed $SmC_{TB\text{-}SH}$ in which SH (single helix) refers to the presence of a short, distorted clock-type helix. In the lower temperature $SmC_{TB\text{-}DH}$ phase, an additional longer helix is superimposed on the short one, and DH denotes double helix. This second helix leads to space-averaging of the azimuthal positions of the molecules when moving along the layer normal in the $SmC_{TB\text{-}DH}$ phase, and thus a homeotropic texture is observed in this phase. On cooling the $SmC_{TB\text{-}DH}$ phase, a weakly birefringent, uncharacteristic texture develops (Fig. 12e), and a chain-like pattern emerged for planar aligned samples.

For all the homologues with $m \geq 12$, the layer spacing, d, corresponds to approximately twice the molecular length, l, in

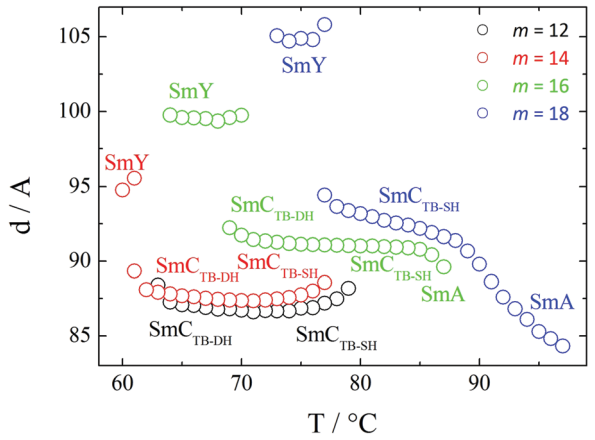

Fig. 14 The temperature dependence of the layer spacings shown for the smectic phases exhibited by the CB10O·*m* homologues with $m \geq 12$.

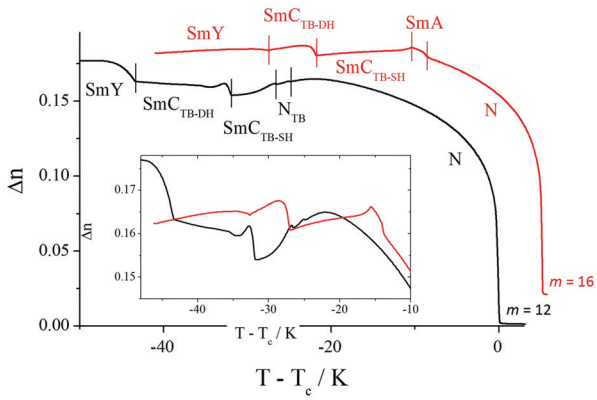

Fig. 16 Optical birefringence as a function of scaled temperature, $T-T_c$ (T_c is the I–N phase transition temperature) for CB10O·12 (black) and CB10O·16 (red). In the inset: a magnified section highlighting the dependence of the birefringence around the SmC_{TB} temperature range.

all the smectic phases (Fig. 14). In the SmA phase, d increases strongly with decreasing temperature, and such behaviour, typical for bent molecules, is often attributed to decreasing interdigitation of the terminal chains between neighbouring layers. By comparison, the temperature dependence of d is much less pronounced in the smectic C_{TB} phases. It is noteworthy that there is no noticeable change in the layer spacing at the $SmC_{TB\text{-}SH}$–$SmC_{TB\text{-}DH}$ transition implying that the tilt angle in both phases must be similar.

Optical studies revealed typical behaviour for the change in optical birefringence at the N–N_{TB} phase transition. Specifically, the birefringence decreases in the twist-bend nematic phase due to the tilting of the molecules with respect to the helix axis, and the azimuthal averaging of the molecular positions, see Fig. 15. At the transition to the SmC_A phase, the birefringence increases discontinuously because of the coupling of orientational order to positional order.

For longer homologues (Fig. 16), the N-SmA phase transition is accompanied by a slight increase in the birefringence arising from an increase in the orientational order parameter associated with layer formation. The onset of the $SmC_{TB\text{-}SH}$ phase is accompanied by a decrease in the birefringence due to the tilting of the molecules and the formation of short helices with a distorted-clock structure, *i.e.*, the phase is biaxial. The transition from the biaxial $SmC_{TB\text{-}SH}$ phase to the uniaxial $SmC_{TB\text{-}DH}$ phase causes a step-like increase in the measured birefringence for planar cells with a book-shelf geometry in which the molecules in the $SmC_{TB\text{-}SH}$ phase are preferentially tilted in the sample plane whereas in the $SmC_{TB\text{-}DH}$ phase the additional helix causes the full averaging of the molecular positions on the tilt cone. For the homologues m = 12 and 14 an almost continuous decrease of the birefringence is found across the N_{TB} and $SmC_{TB\text{-}SH}$ phases.

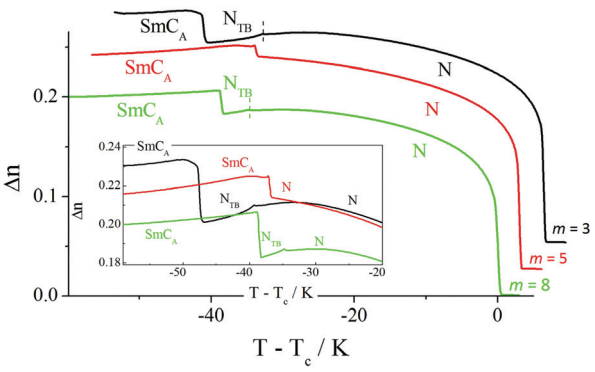

Fig. 15 Optical birefringence as a function of scaled temperature, $T-T_c$ (T_c is the I–N phase transition temperature), for selected CB10O·*m* homologues. In the inset: a magnified section highlighting the changes in Δn at the transition to the N_{TB} and SmC_A phases.

We now return to consider the unprecedented pattern of phase behaviour seen in Fig. 2. Short (m = 2,3) and intermediate (m = 8–14) homologues exhibit the N_{TB} phase, whereas for the homologues with m = 4–8, 16 and 18, Sm–N phase transitions are observed, and N_{TB} behaviour is extinguished. It is striking that the nature of the smectic phase is very different between the homologues with m = 3–8 that exhibit an anticlinic smectic C_A phase, and those with m = 12–18 that show twist-bend smectic phases. These two regions of such differing smectic behaviour are separated by two homologues, m = 9,10, for which no smectic behaviour is observed.

If we first consider the behaviour of the homologues with $m \leq 8$, Fig. 17 shows a magnified section of a phase diagram, constructed using transition temperatures taken from birefringence measurements performed under identical conditions for a selected range of dimers. T_{NI} and $T_{N_{TB}N}$ decrease on increasing m essentially in a linear manner with a weak odd–even effect superimposed. Similar behaviour has been observed for other series of non-symmetric dimers[49,54,55] and interpreted in terms of the increasing dilution of the interactions between mesogenic units arising from the increased volume fraction of alkyl chains. The superimposed weak alternation is attributed to the change in average molecular shape associated with varying the parity of the terminal chain. By comparison to the linear dependence of T_{NI} and $T_{N_{TB}N}$ on m, the temperature at which the SmC_A phase is formed by the homologues with

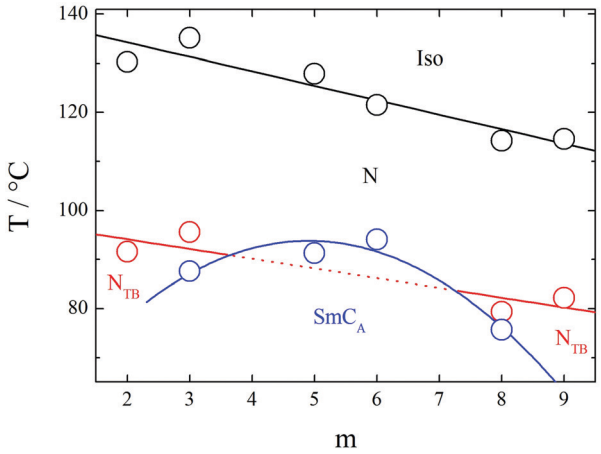

Fig. 17 A magnified section of the phase diagram shown in Fig. 2 for the CB10O·*m* series for selected homologues in the range *m* = 2–9. The transition temperatures are fitted either to a linear (Iso–N, N–N_{TB}) or parabolic dependence (N,N_{TB}–SmC_A) on *m*. The dotted line shows the virtual N–N_{TB} phase transition which is not observed because of the enhanced stability of the SmC_A phase for intermediate homologues. A SmC_A phase is not observed for *m* = 2 and 9.

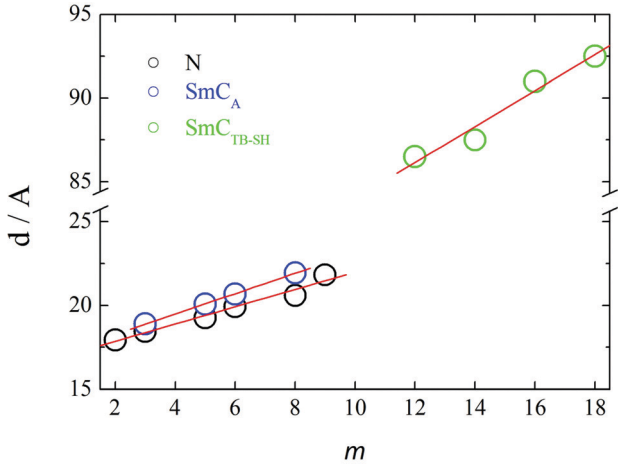

Fig. 18 The layer spacings in the smectic phases (SmC_A (blue); SmC_{TB-SH} (green)) and the periodicities corresponding to the broad low angle diffraction signal in the nematic phase (black) for the CB10O·*m* series.

m = 3–8, from either the N or N_{TB} phase, shows a parabolic dependence on *m*. The SmC_A phase appears most stable for homologues in which the length of the terminal chain, *m*, is around half the length of the flexible spacer. This ratio leads to the ideal conditions for the separation of the mesogenic aromatic cores and aliphatic chains in the intercalated smectic structure sketched in Fig. 7. This separation is thought to be driven by a favourable specific interaction between the unlike mesogenic units suggested to be an electrostatic quadrupolar interaction between groups with quadrupole moments which are opposite in sign.[56] If the terminal chain is either considerably shorter or longer than half the spacer, then the arrangement of the molecules into an intercalated lamellar structure is less favourable and twist-bend nematic behaviour is restored. This pattern of behaviour has not previously been reported. Induced smectic behaviour has been observed on mixing two twist-bend nematogens but not to the exclusion of the twist-bend nematic phase.[57]

It is important to note that for terminal chain lengths *m* = 1–10, in both the N and N_{TB} phases, the broad low-angle signal in the X-ray diffraction patterns correspond to a short-range intercalated structure and no evidence was found for an additional density wave having a periodicity corresponding to the full molecular length, see Fig. 18. This is quite unlike the behaviour seen for the related CB6O·*m* and CB6O·Om series for which frustrated packing arrangements were observed for intermediate chain lengths.[49,54] The layer spacing in the smectic C_A phase and the mean distance in the nematic phase grow monotonically on increasing the terminal chain length, *m*, with the coefficient 0.5–0.6 Å per additional carbon atom (Fig. 18). This provides further evidence supporting the assignment of an intercalated arrangement of the molecules as shown in Fig. 7, given that for a structure with a single molecule per smectic layer a coefficient of twice this value would be expected. Furthermore, an approximately equimolar mixture of the homologues with *m* = 3 and 9 showed only nematic phases over a broad temperature range, and no smectic behaviour was observed prior to crystallization at around room temperature. This suggests that in the mixture, the smectic phase shown by CB10O·3 is destabilized in favour of nematic (N and N_{TB}) phases implying that the energy balance between lamellar and nematic structures is weak.

On increasing the terminal chain length, $m \geq 12$, the local structure in the smectic layers and in the nematic phases becomes interdigitated, and the respective layer spacing or mean distance is approximately 2*l*, see Fig. 18. The terminal chains in these dimers are too long to be accommodated within an intercalated arrangement, and the bilayer-type interdigitated structure is driven, at least to some extent, by anti-parallel associations between the polar and polarisable cyanobiphenyl groups while smectic phase behaviour may be attributed to the molecular inhomogeneity arising from the long alkyl chains.[46,48] It is interesting to note that the switch in the local packing within the nematic phase is not apparent in the dependence of T_{NI} on *m*, see Fig. 2, and again this has been observed for related series.[49,54] An approximately equimolar mixture of the homologues with *m* = 6 and 16, *i.e.*, two homologues forming smectic phases directly below the nematic phase, exhibited the N_{TB} phase over a broad temperature range, and the SmY phase. This reveals an incompatibility between the intercalated and interdigitated bilayer-type smectic variants, and these are destabilised in the mixture revealing the underlying N_{TB} phase.

Finally, in the middle of the phase diagram the homologues with *m* = 9 and 10 show only N and N_{TB} phases in which the local structure has an intercalated arrangement. This suggests that although dynamic associations between the unlike mesogenic units, presumably driven by the favourable specific interaction described earlier, lead to the formation of fluctuating, short-range intercalated structures, the long terminal chains destabilise lamellar packing.

Conclusions

It is well-established that the liquid crystalline behaviour of non-symmetric dimers such as the CB*n*O·*m* series consisting of two mesogenic units that exhibit a favourable specific interaction is determined largely by the relative lengths of the flexible spacer, *n*, and terminal chain, *m*.[50] If $m/n \lesssim 0.5$ then a tendency to form intercalated structures is normally observed driven by the interaction between the unlike groups, and as *m* increases such that $m \gtrsim n$, bilayer structures are formed with the polar groups accommodated between every second sublayer. Such behaviour is reported here for the CB10O·*m* series but the inherently bent shape of these dimers combined with their long spacer have given rise to the overlay of a novel pattern of phase behaviour superimposed onto this rather general behaviour. Specifically, an intercalated SmC_A phase is observed if $m/11 \approx 0.5$ and on either side of this condition an N_{TB} phase is seen. As *m* increases such that $m \gtrsim 11$ and the molecules are no longer able to form intercalated structures, bilayer-type SmA and two tilted smectic phases with helical structures are observed, the biaxial $SmC_{TB\text{-}SH}$ and the uniaxial $SmC_{TB\text{-}DH}$ phases and these are shown schematically in Fig. 13.

Conflicts of interest

There are no conflicts to declare.

Acknowledgements

A. F. A. wishes to thank the Ministry of Education and the University of Hail, Saudi Arabia through the Cultural Bureau of Saudi Arabia, London for their financial support during the study period. E. G. and D. P. thank the National Science Centre (Poland) for financial support under the grant no. 2016/22/A/ST5/00319.

References

1 M. Cestari, S. Diez-Berart, D. A. Dunmur, A. Ferrarini, M. R. de la Fuente, D. J. B. Jackson, D. O. Lopez, G. R. Luckhurst, M. A. Perez-Jubindo, R. M. Richardson, J. Salud, B. A. Timimi and H. Zimmermann, Phase behavior and properties of the liquid-crystal dimer 1″,7″-bis(4-cyanobiphenyl-4′-yl) heptane: A twist-bend nematic liquid crystal, *Phys. Rev. E: Stat., Nonlinear, Soft Matter Phys.*, 2011, **84**, 031704.

2 V. Borshch, Y. K. Kim, J. Xiang, M. Gao, A. Jakli, V. P. Panov, J. K. Vij, C. T. Imrie, M. G. Tamba, G. H. Mehl and O. D. Lavrentovich, Nematic twist-bend phase with nanoscale modulation of molecular orientation, *Nat. Commun.*, 2013, **4**, 2635.

3 D. Chen, J. H. Porada, J. B. Hooper, A. Klittnick, Y. Shen, M. R. Tuchband, E. Korblova, D. Bedrov, D. M. Walba, M. A. Glaser, J. E. Maclennan and N. A. Clark, Chiral heliconical ground state of nanoscale pitch in a nematic liquid crystal of achiral molecular dimers, *Proc. Natl. Acad. Sci. U. S. A.*, 2013, **110**, 15931–15936.

4 I. Dozov, On the spontaneous symmetry breaking in the mesophases of achiral banana-shaped molecules, *Europhys. Lett.*, 2001, **56**, 247–253.

5 R. Walker, D. Pociecha, J. M. D. Storey, E. Gorecka and C. T. Imrie, The Chiral Twist-Bend Nematic Phase (N*(TB)), *Chem. – Eur. J.*, 2019, **25**, 13329–13335.

6 J. P. Abberley, R. Killah, R. Walker, J. M. D. Storey, C. T. Imrie, M. Salamonczyk, C. H. Zhu, E. Gorecka and D. Pociecha, Heliconical smectic phases formed by achiral molecules, *Nat. Commun.*, 2018, **9**, 228.

7 M. Salamonczyk, N. Vaupotic, D. Pociecha, R. Walker, J. M. D. Storey, C. T. Imrie, C. Wang, C. H. Zhu and E. Gorecka, Multilevel chirality in liquid crystals formed by achiral molecules, *Nat. Commun.*, 2019, **10**, 1922.

8 J. K. Vij, Y. P. Panarin, S. P. Sreenilayam, M. Alaasar and C. Tschierske, Investigation of the heliconical smectic SmCSPFhel phase in achiral bent-core mesogens derived from 4-cyanoresorcinol, *Phys. Rev. Mater.*, 2019, **3**, 045603.

9 S. P. Sreenilayam, Y. P. Panarin, J. K. Vij, V. P. Panov, A. Lehmann, M. Poppe, M. Prehm and C. Tschierske, Spontaneous helix formation in non-chiral bent-core liquid crystals with fast linear electro-optic effect, *Nat. Commun.*, 2016, **7**, 11369.

10 D. Pociecha, N. Vaupotic, M. Majewska, E. Cruickshank, R. Walker, J. M. D. Storey, C. T. Imrie, C. Wang and E. Gorecka, Photonic band gap in achiral liquid crystals – a twist on a twist, *Adv. Mater.*, 2021, **33**, 2103288.

11 P. A. Henderson and C. T. Imrie, Methylene-linked liquid crystal dimers and the twist-bend nematic phase, *Liq. Cryst.*, 2011, **38**, 1407–1414.

12 R. J. Mandle, E. J. Davis, C. C. A. Voll, C. T. Archbold, J. W. Goodby and S. J. Cowling, The relationship between molecular structure and the incidence of the N-TB phase, *Liq. Cryst.*, 2015, **42**, 688–703.

13 D. A. Paterson, R. Walker, J. P. Abberley, J. Forestier, W. T. A. Harrison, J. M. D. Storey, D. Pociecha, E. Gorecka and C. T. Imrie, Azobenzene-based liquid crystal dimers and the twist-bend nematic phase, *Liq. Cryst.*, 2017, **44**, 2060–2078.

14 R. J. Mandle, C. T. Archbold, J. P. Sarju, J. L. Andrews and J. W. Goodby, The Dependency of Nematic and Twist-bend Mesophase Formation on Bend Angle, *Sci. Rep.*, 2016, **6**, 36682.

15 E. Cruickshank, M. Salamonczyk, D. Pociecha, G. J. Strachan, J. M. D. Storey, C. Wang, J. Feng, C. H. Zhu, E. Gorecka and C. T. Imrie, Sulfur-linked cyanobiphenyl-based liquid crystal dimers and the twist-bend nematic phase, *Liq. Cryst.*, 2019, **46**, 1595–1609.

16 C. T. Archbold, J. L. Andrews, R. J. Mandle, S. J. Cowling and J. W. Goodby, Effect of the linking unit on the twist-bend nematic phase in liquid crystal dimers: a comparative study of two homologous series of methylene- and ether-linked dimers, *Liq. Cryst.*, 2017, **44**, 84–92.

17 J. P. Abberley, J. M. D. Storey and C. T. Imrie, Structure-property relationships in azobenzene-based twist-bend nematogens, *Liq. Cryst.*, 2019, **46**, 2102–2114.

18 R. J. Mandle, Designing Liquid-Crystalline Oligomers to Exhibit Twist-Bend Modulated Nematic Phases, *Chem. Rec.*, 2018, **18**, 1341–1349.
19 R. Walker, M. Majewska, D. Pociecha, A. Makal, J. M. D. Storey, E. Gorecka and C. T. Imrie, Twist-Bend Nematic Glasses: The Synthesis and Characterisation of Pyrene-based Nonsymmetric Dimers, *ChemPhysChem*, 2021, **22**, 461–470.
20 V. P. Panov, J. K. Vij and G. H. Mehl, Twist-bend nematic phase in cyanobiphenyls and difluoroterphenyls bimesogens, *Liq. Cryst.*, 2017, **44**, 147–159.
21 D. A. Paterson, M. Gao, Y. K. Kim, A. Jamali, K. L. Finley, B. Robles-Hernandez, S. Diez-Berart, J. Salud, M. R. de la Fuente, B. A. Timimi, H. Zimmermann, C. Greco, A. Ferrarini, J. M. D. Storey, D. O. Lopez, O. D. Lavrentovich, G. R. Luckhurst and C. T. Imrie, Understanding the twist-bend nematic phase: the characterisation of 1-(4-cyanobiphenyl-4′-yloxy)-6-(4-cyanobiphenyl-4′-yl)hexane (CB6OCB) and comparison with CB7CB, *Soft Matter*, 2016, **12**, 6827–6840.
22 K. Merkel, B. Loska, C. Welch, G. H. Mehl and A. Kocot, The role of intermolecular interactions in stabilizing the structure of the nematic twist-bend phase, *RSC Adv.*, 2021, **11**, 2917–2925.
23 J. P. Abberley, R. Walker, J. M. D. Storey and C. T. Imrie, Molecular structure and the twist-bend nematic phase: the role of terminal chains, *Liq. Cryst.*, 2020, **47**, 1232–1245.
24 A. Knezevic, I. Dokli, J. Novak, D. Kontrec and A. Lesac, Fluorinated twist-bend nematogens: the role of intermolecular interaction, *Liq. Cryst.*, 2021, **48**, 756–766.
25 E. Forsyth, D. A. Paterson, E. Cruickshank, G. J. Strachan, E. Gorecka, R. Walker, J. M. D. Storey and C. T. Imrie, Liquid crystal dimers and the twist-bend nematic phase: On the role of spacers and terminal alkyl chains, *J. Mol. Liq.*, 2020, **320**, 114391.
26 A. Lesac, U. Baumeister, I. Dokli, Z. Hamersak, T. Ivsic, D. Kontrec, M. Viskic, A. Knezevic and R. J. Mandle, Geometric aspects influencing N-N-TB transition - implication of intramolecular torsion, *Liq. Cryst.*, 2018, **45**, 1101–1110.
27 Y. Arakawa, K. Komatsu, T. Shiba and H. Tsuji, Methylene- and thioether-linked cyanobiphenyl-based liquid crystal dimers CBnSCB exhibiting room temperature twist-bend nematic phases and glasses, *Mater. Adv.*, 2021, **2**, 1760–1773.
28 Y. Arakawa, K. Komatsu, Y. Ishida and H. Tsuji, Thioether-linked azobenzene-based liquid crystal dimers exhibiting the twist-bend nematic phase over a wide temperature range, *Liq. Cryst.*, 2021, **48**, 641–652.
29 Y. Arakawa, K. Komatsu and H. Tsuji, Twist-bend nematic liquid crystals based on thioether linkage, *New J. Chem.*, 2019, **43**, 6786–6793.
30 R. J. Mandle and J. W. Goodby, A Nanohelicoidal Nematic Liquid Crystal Formed by a Non-Linear Duplexed Hexamer, *Angew. Chem., Int. Ed.*, 2018, **57**, 7096–7100.
31 F. P. Simpson, R. J. Mandle, J. N. Moore and J. W. Goodby, Investigating the Cusp between the nano-and macro-sciences in supermolecular liquid-crystalline twist-bend nematogens, *J. Mater. Chem. C*, 2017, **5**, 5102–5110.
32 R. J. Mandle, M. P. Stevens and J. W. Goodby, Developments in liquid-crystalline dimers and oligomers, *Liq. Cryst.*, 2017, **44**, 2046–2059.
33 R. J. Mandle and J. W. Goodby, A Liquid Crystalline Oligomer Exhibiting Nematic and Twist-Bend Nematic Mesophases, *ChemPhysChem*, 2016, **17**, 967–970.
34 Y. Arakawa, K. Komatsu, S. Inui and H. Tsuji, Thioether-linked liquid crystal dimers and trimers: The twist-bend nematic phase, *J. Mol. Struct.*, 2020, 1199.
35 Y. Arakawa, K. Komatsu, T. Shiba and H. Tsuji, Phase behaviors of classic liquid crystal dimers and trimers: Alternate induction of smectic and twist-bend nematic phases depending on spacer parity for liquid crystal trimers, *J. Mol. Liq.*, 2021, **326**, 115319.
36 M. R. Tuchband, D. A. Paterson, M. Salamonczykc, V. A. Norman, A. N. Scarbrough, E. Forsyth, E. Garcia, C. Wang, J. M. D. Storey, D. M. Walba, S. Sprunt, A. Jakli, C. H. Zhu, C. T. Imrie and N. A. Clark, Distinct differences in the nanoscale behaviors of the twist-bend liquid crystal phase of a flexible linear trimer and homologous dimer, *Proc. Natl. Acad. Sci. U. S. A.*, 2019, **116**, 10698–10704.
37 D. Chen, M. Nakata, R. Shao, M. R. Tuchband, M. Shuai, U. Baumeister, W. Weissflog, D. M. Walba, M. A. Glaser, J. E. Maclennan and N. A. Clark, Twist-bend heliconical chiral nematic liquid crystal phase of an achiral rigid bent-core mesogen, *Phys. Rev. E: Stat., Nonlinear, Soft Matter Phys.*, 2014, **89**, 022506.
38 S. P. Sreenilayam, V. P. Panov, J. K. Vij and G. Shanker, The N-TB phase in an achiral asymmetrical bent-core liquid crystal terminated with symmetric alkyl chains, *Liq. Cryst.*, 2017, **44**, 244–253.
39 S. M. Jansze, A. Martinez-Felipe, J. M. D. Storey, A. T. M. Marcelis and C. T. Imrie, A Twist-Bend Nematic Phase Driven by Hydrogen Bonding, *Angew. Chem., Int. Ed.*, 2015, **54**, 643–646.
40 R. Walker, D. Pociecha, M. Salamonczyk, J. M. D. Storey, E. Gorecka and C. T. Imrie, Supramolecular liquid crystals exhibiting a chiral twist-bend nematic phase, *Mater. Adv.*, 2020, **1**, 1622–1630.
41 R. Walker, D. Pociecha, C. A. Crawford, J. M. D. Storey, E. Gorecka and C. T. Imrie, Hydrogen bonding and the design of twist-bend nematogens, *J. Mol. Liq.*, 2020, **303**, 112630.
42 R. Walker, D. Pociecha, A. Martinez-Felipe, J. M. D. Storey, E. Gorecka and C. T. Imrie, Twist-Bend Nematogenic Supramolecular Dimers and Trimers Formed by Hydrogen Bonding, *Crystals*, 2020, **10**, 175.
43 R. Walker, D. Pociecha, J. P. Abberley, A. Martinez-Felipe, D. A. Paterson, E. Forsyth, G. B. Lawrence, P. A. Henderson, J. M. D. Storey, E. Gorecka and C. T. Imrie, Spontaneous chirality through mixing achiral components: a twist-bend nematic phase driven by hydrogen-bonding between unlike components, *Chem. Commun.*, 2018, **54**, 3383–3386.

44 C. T. Imrie, P. A. Henderson and G.-Y. Yeap, Liquid crystal oligomers: going beyond dimers, *Liq. Cryst.*, 2009, **36**, 755–777.
45 G. S. Attard, S. Garnett, C. G. Hickman, C. T. Imrie and L. Taylor, Asymmetric dimeric liquid-crystals with charge-transfer groups, *Liq. Cryst.*, 1990, **7**, 495–508.
46 C. T. Imrie, Non-symmetric liquid crystal dimers: How to make molecules intercalate, *Liq. Cryst.*, 2006, **33**, 1449–1454.
47 J. L. Hogan, C. T. Imrie and G. R. Luckhurst, Asymmetric dimeric liquid-crystals - the preparation and properties of the α-(4-cyanobiphenyl-4′-oxy)-ω-(4-*n*-alkylanilinebenzylidene-4′-oxy)hexanes, *Liq. Cryst.*, 1988, **3**, 645–650.
48 G. S. Attard, R. W. Date, C. T. Imrie, G. R. Luckhurst, S. J. Roskilly, J. M. Seddon and L. Taylor, Nonsymmetrical dimeric liquid-crystals - the preparation and properties of the alpha-(4-cyanobiphenyl-4′-yloxy)-omega-(4-*n*-alkylanilinebenzylidene-4′-oxy)alkanes, *Liq. Cryst.*, 1994, **16**, 529–581.
49 R. Walker, D. Pociecha, G. J. Strachan, J. M. D. Storey, E. Gorecka and C. T. Imrie, Molecular curvature, specific intermolecular interactions and the twist-bend nematic phase: the synthesis and characterisation of the 1-(4-cyanobiphenyl-4-yl)-6-(4-alkylanilinebenzylidene-4-oxy)hexanes (CB6O·*m*), *Soft Matter*, 2019, **15**, 3188–3197.
50 C. T. Imrie and P. A. Henderson, Liquid crystal dimers and higher oligomers: Between monomers and polymers, *Chem. Soc. Rev.*, 2007, **36**, 2096–2124.
51 D. A. Paterson, J. P. Abberley, W. T. Harrison, J. M. Storey and C. T. Imrie, Cyanobiphenyl-based liquid crystal dimers and the twist-bend nematic phase, *Liq. Cryst.*, 2017, **44**, 127–146.
52 C. J. Gibb, J. M. D. Storey and C. T. Imrie, Synthesis and characterisation of the ω-bromo-1-(4-cyanobiphenyl-4′-yl) alkanes (CBnBr), *Liq. Cryst.*, 2022, DOI: **10.1080/02678292.2022.2084568**.
53 R. Pindak, D. E. Moncton, S. C. Davey and J. W. Goodby, X-ray-observation of a stacked hexatic liquid-crystal B-phase, *Phys. Rev. Lett.*, 1981, **46**, 1135–1138.
54 D. A. Paterson, C. A. Crawford, D. Pociecha, R. Walker, J. M. D. Storey, E. Gorecka and C. T. Imrie, The role of a terminal chain in promoting the twist-bend nematic phase: the synthesis and characterisation of the 1-(4-cyanobiphenyl-4′-yl)-6-(4-alkyloxyanilinebenzylidene-4′-oxy)hexanes, *Liq. Cryst.*, 2018, **45**, 2341–2351.
55 R. Walker, D. Pociecha, J. M. D. Storey, E. Gorecka and C. T. Imrie, Remarkable smectic phase behaviour in odd-membered liquid crystal dimers: the CT6O·*m* series, *J. Mater. Chem. C*, 2021, **9**, 5167–5173.
56 A. E. Blatch, I. D. Fletcher and G. R. Luckhurst, The intercalated smectic-a phase - the liquid-crystal properties of the alpha(4-cyanobiphenyl-4′-yloxy)-omega-(4-alkyloxycinnamoate)alkanes, *Liq. Cryst.*, 1995, **18**, 801–809.
57 A. Knezevic, I. Dokli, M. Sapunar, S. Segota, U. Baumeister and A. Lesac, Induced smectic phase in binary mixtures of twist-bend nematogens, *Beilstein J. Nanotechnol.*, 2018, **9**, 1297–1307.

